BiEOP: A Bistable, Soft Actuator Driven by Electroosmotic Pumps

Tianyu Yu, Hajun Lee, and Lining Yao*

***Abstract*— Bistable actuators have provided unique advantages for soft robotics, such as reconfigurable shape or multifunctional behaviors. However, achieving self-contained and controllable bistable actuation still remains challenging. In this work, we present BiEOP, a bistable soft actuator driven by electroosmotic pumps (EOPs). BiEOP consists of two symmetric, dome-shaped elastic shells separated by an EOP layer, which transfers internal working liquid under electrical actuation below 300 V to switch between the actuator's bistable configurations. We analyze and experimentally validate its bistable behavior based on the pressure–volume characterization of the elastic shell. We then demonstrate a soft robot composed of multiple BiEOP modules that reconfigures its body shape to switch between bristle locomotion and surface adhesion functions. This reconfigurability enables diverse functional behaviors, such as remaining stationary in windy environments or picking up and transporting flake samples for pipe inspection. We envision BiEOP as a modular actuator capable of inducing shape reconfiguration and multifunctionality in the design of future soft robots.**

I. INTRODUCTION

A bistable structure is a mechanical system exhibiting two stable configurations in one body, which exhibit distinctive behaviors due to their ability to switch between different stable configurations via snap-through transitions [1]. This unique mechanical behavior not only plays a crucial role in natural systems, such as in Venus flytraps [2], but has also been widely adopted in recent robotic research fields, such as soft robot design [3], to exploit the diverse advantages offered by bistability. For example, soft robots can achieve reconfigurable form factors and functionalities by assembling multiple bistable modules or embedding structures with multistability [4], [5]. Also, from the perspective of energy efficiency and control simplicity, bistable structures are highly promising, as they typically consume energy to overcome the energy boundary for triggering the snap-through transitions, without requiring continuous input to maintain a stable configuration [6].

Towards this motivation, researchers have explored diverse actuation mechanisms to realize bistable actuation in soft robotics. Pneumatic systems are one of the most representative approaches [7], [8]. They provide high power output and precise controllability, but usually rely on bulky external mechanical pumps and regulators to control the pneumatic flow. Other emerging technologies include using smart materials that respond to external stimuli, such as magnetic or optical actuation, to enable soft robots with untethered contoll [9], [10]. However, these systems typically depend on specialized environmental setups, which may constrain their deployment in real-world applications. Shape Memory Alloys (SMAs) and Shape Memory Polymers (SMPs) are other types of smart materials that are capable of shape changes when actuated by integrated heating elements within compact, self-contained structures. However, they usually face challenges in realizing complex morphologies and alleviating heat accumulation [11], [12]. Other stimuli-responsive systems, such as thermo-, hygro-, and pH-responsive materials, enable independent actuation without the need for external controllers [13]–[15], but they typically suffer from limited controllability and slow response times. In contrast to the aforementioned methods, electroactive materials present emerging opportunities, which can induce deformation or fluid motion under an applied electric field via embedded electrodes. These systems, such as dielectric elastomer actuators (DEAs) [16], offer the potential for self-contained, fully soft, and highly controllable actuation, providing a promising pathway to further expand the functional and morphological design space of soft robotics.

Electroosmotic pump (EOP) is another technique that utilizes electrokinetic fluidic materials to generate hydraulic flow or pressure from electrical power directly. The working principle of an EOP relies on the electrical double layer (EDL) naturally formed at the nanometer-scale interface between a fluid and the capillary surfaces of the pump membrane [17]. When an external electric field is applied, the charges in the EDL experience Coulombic forces that drag the surrounding fluid through viscous interactions, resulting in electroosmotic pressure and flow [18]. Compared to other electroactive material systems, such as DEAs or hydraulically amplified self-healing electrostatic (HASEL) actuators [19], it has the potential to actuate diverse morphologies by inducing electrokinetic flow in fluidic systems with versatile form factors [20]. Besides, the EOP also operates at a relatively low voltage (typically below 1 kV) compared to other electro-hydraulic devices, such as Electrohydrodynamic (EHD) pumps [21], [22]. Previous works have explored using EOPs to construct continuously driven actuators for applications such as tactile displays [23] or shape-changing actuators [24]. However, these actuators typically exhibit single-stable state, meaning that deformation only occurs under continuous electrical input and reverts once the power is removed. Inspired by pneumatic bistable actuators [7], we explore the use of EOP-driven liquid transfer to actuate bistable dome-shaped elastic shells, creating bistable, soft actuators.

We present BiEOP, a bistable soft actuator driven by electroosmotic pumps. It comprises two symmetric dome-

All authors are with the Morphing Matter Lab, Department of Mechanical Engineering, UC Berkeley, Berkeley, California, USA

*Corresponding author: liningy@berkeley.edu

shaped elastic shells separated by an EOP layer, which transfers internal working liquid under electrical actuation to switch between the actuator's bistable configurations. We analyze and experimentally validate the actuator's bistable behavior based on the pressure–volume characterization of the elastic shell. Furthermore, We demonstrate a soft robot composed of multiple BiEOP modules that reconfigures its body shape to switch between bristle locomotion and surface adhesion functions. This reconfigurability enables diverse functional behaviors, such as remaining stationary in windy environments or picking up and transporting flake samples for pipe inspection. We envision BiEOP as a modular actuator capable of inducing shape reconfiguration and multifunctionality in the design of future soft robots.

II. DESIGN AND FABRICATION

The BiEOP actuator is constructed around a flexible EOP serving as the middle layer, with two mirror-symmetric dome-shaped elastic shells attached to its top and bottom faces (Figure 1a). The actuator is filled with a fixed volume of working liquid, maintaining one shell in a convex configuration and the other in a concave configuration. When actuated, a voltage is applied to the EOP to pump the working liquid from the convex shell toward the concave shell, inverting their geometries and switching the actuator from one stable state to the other (Figure 1b). Reversing the voltage polarity reverses the morphing direction. The detailed components and their fabrication procedures are introduced below.

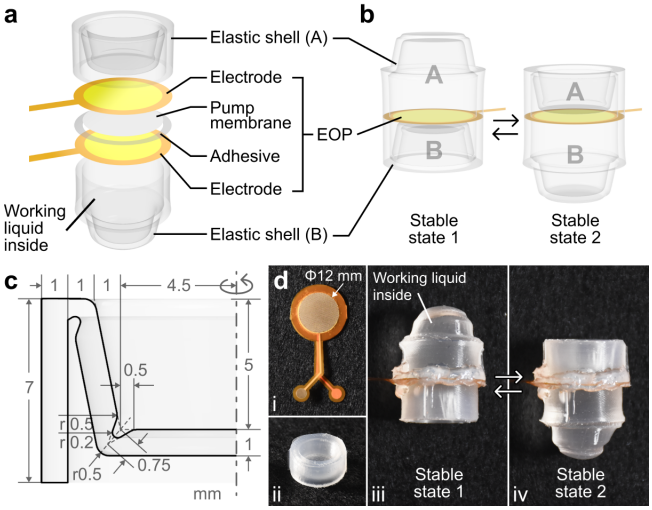

Fig. 1. Design of BiEOP actuator. (a) Structural composition. (b) Two stable states of the actuator. (c) Mechanical design of the elastic shell. (d) Real photos of (i) the assembled EOP, (ii) the elastic shell, and (iii-iv) two stable states of the actuator.

A. Electroosmotic Pump (EOP)

The middle EOP layer comprises two symmetric electrodes that sandwich a pumping membrane and a double-sided adhesive layer. Each electrode features a 12 mm-diameter circular pumping region, with a via array designed according to prior work [20] to facilitate fluid transport. A bonding region at least 2 mm wide surrounds the pumping area to ensure reliable sealing. The electrodes are implemented using double-sided flexible printed circuits (FPCs) by an industrial manufacturer (JLCPCB) based on custom CAD layouts. The pumping membrane and adhesion layer are designed and fabricated following the same procedures as in [20]. Figure 1d shows a fully assembled EOP layer, where all components are manually aligned and laminated via a pick-and-place process. To actuate the pump, we followed previous work [20], [24], where a voltage below 300 V is generated by a DC converter and then applied to the pump under the control of Arduino boards and relays.

B. Elastic Shell

The upper and lower elastic shells are designed to exhibit snap-through transition behavior, providing the actuator with bistable configurations. As illustrated in Figure 1c, each shell adopts a dome-shaped geometry that can switch between convex and concave shapes. Grooves are designed along the inward-turning edges of the dome structure to enhance the snapping behavior. An outer wall surrounds the dome to facilitate bonding with the middle EOP layer. Except for the groove structure, the thickness of the shell is 1 mm everywhere. The shells are then fabricated by casting Smooth-On Sorta-Clear 12 silicone into 3D-printed molds, and all shells are initially cast in the concave shape configuration (Figure 1d). During assembly, Smooth-on Sil-Poxy glue is applied along the rim of the shell wall or the edge of the EOP electrodes, and the components are manually aligned and bonded together to complete the assembly.

C. Working Liquid

We use propylene carbonate as the working liquid inside the actuator [20]. We use a syringe with a 30G needle to first evacuate the air inside each actuator and then inject the working fluid. When required, we use Sil-Poxy glue to seal any leakage points. A fully assembled BiEOP actuator and its two stable states are shown in Figure 1d.

The total volume of working liquid injected into the actuator consists of two parts: (1) V_s — the inherent cavity volume enclosed between the concave shell and its base, which can be theoretically calculated. For one shell, this volume is approximately 274 μL. (2) V_t — the additional transferable liquid volume that allows fluid exchange between the two shells and ensures that either shell can maintain a convex configuration. This value was determined empirically from experimental observation and is 1100 μL (see analysis in Section III-B). Therefore, the total liquid volume added to a single actuator is $2V_s + V_t \approx 1.6$ mL.

III. EXPERIMENT

In this section, we first characterized the pressure–volume performance of a single shell through experiments. Based on the experiment data, we then analyzed and experimentally validated the bistable behavior of a dual-shell actuator.

A. Pressure-volume Characterization of the Elastic Shell

1) Experiment Method: In this experiment, we characterized the pressure–volume performance of a single shell during inflation and deflation of the working liquid. The experimental setup is illustrated in Figure 2a. A single shell was fixed to a 3D-printed rigid connector, which was tightly bonded to the shell wall and constrained the wall's deformation. A 3D-printed indicator was glued to the center of the shell to visualize the shape transitions, which also simulated the other components potentially mounted at the same position in practical applications. A syringe pump was connected to the connector via a silicone tube to inflate and deflate the test shell at a controllable low speed. The entire fluidic system was filled with propylene carbonate as the working liquid. A pressure sensor (Adafruit MPRLS Ported Pressure Sensor) was connected to the fluidic line to measure the internal gauge pressure of the system above the atmosphere pressure level. We assumed that the system operated under quasi-static conditions, such that the static pressure could be considered uniform throughout the fluidic system.

During the experiment, the test shell underwent multiple inflate–deflate cycles at a flow rate of 6.67 mL/min, with each inflation or deflation phase lasting 13.5 s. Six repeated cycles were conducted continuously. Pressure data were recorded at 10 Hz using a PC, and the volume change was estimated based on the operating time of the syringe pump. A video camera was also used to record the shell's shape-changing process.

2) Results: The pressure-volume performance of the test shell is shown in the plot in Figure 2b. By comparing the curve in the plot with the recorded video of shape changes, we identify two equilibrium points, corresponding to the convex and concave stable configurations of the shell, respectively. Between these two equilibrium points lies the snap-through transition, while the regions outside them represent elastic deformation, including both elastic expansion and contraction.

During the snap-through transition, multiple irregular pressure spikes are observed, which are attributed to the multi-step snapping behaviors during the transition process. In addition, the distinct shapes of the inflation and deflation curves also indicate a hysteretic behavior within an inflation-deflation cycle of the single shell. However, the final volume after one full cycle does not return exactly to its initial value, likely due to accumulated errors in volume estimation. The results of the repeated cycles also show a group of highly consistent pressure–volume curves, suggesting the repeatability and predictability of the performance for one single shell.

B. Bistability of the Dual-shell Actuator

1) Bistability Analysis: Based on the experiment data, we then analyzed the bistable performance of a dual-shell actuator. Specifically, assuming that the working liquid is incompressible, when the volume of one shell changes by ΔV (+ for inflation and - for deflation), the volume of the other shell then changes by $-\Delta V$. Based on this relationship, the pressure responses of the two shells undergoing conjugate volume changes can be plotted on the same coordinate system, as shown in Figure 3.

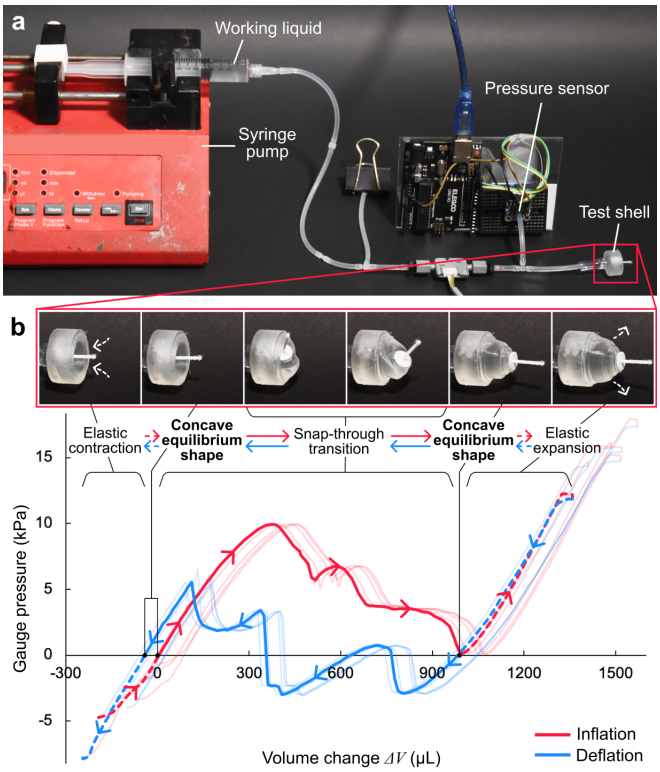

Fig. 2. (a) Experiment setup to characterize the pressure-volume performance of the elastic shell. (b) Results, where the thick solid curves in the plot represent the typical pressure-volume performance during an inflation-deflation cycle. The light curves in the background denote results from other repeated cycles. Captures from the video of the shape-changing process are overlaid on the plot, corresponding to the multiple stages of the curve.

Here, we let the volume change of the *inflating shell* be the horizontal axis. Then, we express the pressure responses of the inflating and deflating shells as follows:

$$P_{in} = P_{in}(\Delta V) \tag{1}$$

$$P_{de} = P_{de}(V_t - \Delta V) \tag{2}$$

where $P_{in}(\cdot)$ and $P_{de}(\cdot)$ correspond to the experimentally measured pressure–volume curves for inflation and deflation shells, respectively (I.e., the red and blue curves in Figure 2b, while both offset-calibrated to set their concave equilibrium points as the original points.) V_t represents the total transferable liquid volume injected during fabrication, which is empirically set to 1100 μL in this analysis.

Based on this configuration, we then derived the pressure difference curve between the two shells as:

$$\Delta P(\Delta V) = P_{in}(\Delta V) - P_{de}(V_t - \Delta V) \tag{3}$$

This $\Delta P(\Delta V)$ curve is also shown in Figure 3, which can be used to describe the state transitions of the actuator system during operation. Based on the $\Delta P(\Delta V)$ curve, we derived the following two inferences:

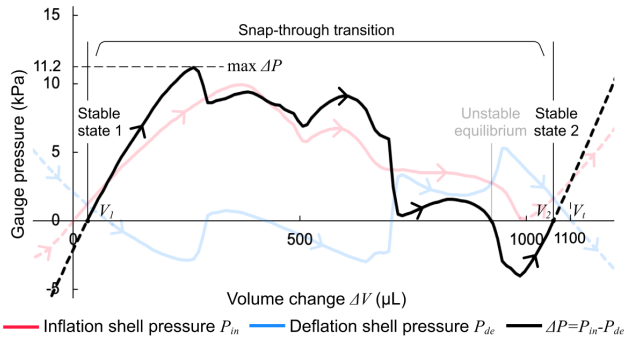

Fig. 3. Bistability analysis of the BiEOP actuator based experimental data. The light red and blue curves denote the pressure-volume performance for the inflation and deflation shells when operating together within a single actuator. The black curve represents the pressure difference between the inflation and the deflation shells. Two stable states are identified on the plot.

(1) The actuator system exhibits two stable states, in which, for each state, one shell performs a convex shape while the other performs a concave shape, or vice versa. We identify these two stable points $(V_1, 0), (V_2, 0)$ on the $\Delta P(\Delta V)$ curve in Figure 3, where

$$\Delta P|_{V_i} = 0 \tag{4}$$

$$\left.\frac{\partial \Delta P}{\partial \Delta V}\right|_{V_i} > 0 \tag{5}$$

$i = 1, 2$. For these two points $(V_1, 0), (V_2, 0)$ that satisfy the above equations, if a small local perturbation occurs at these equilibrium points, e.g., a small increase in ΔV for the inflation shell, then according to Equation 5, ΔP will also increase and then become positive. This indicates the internal pressure of the inflation shell will be larger than that of the deflation shell. As a result, the working liquid tends to flow back into the deflation shell, decreasing the volume of the inflation shell and restoring the system to its equilibrium state.

(2) The threshold pressure that the EOP needs to trigger state switching can be estimated as follows:

$$P_{EOP} > \max \Delta P \tag{6}$$

This is because the pressure difference ΔP between two shells, at any given moment, also represents the pressure threshold the EOP must overcome in order to transfer the working liquid from the deflation shell to the inflation shell. Therefore, only when the pumping pressure of the EOP P_{EOP} exceeds the maximum value of the pressure difference ΔP, can the actuator switch from one stable state to the other. From Figure 3, we estimated $\max \Delta P \approx 11.2$ kPa. According to previous studies that use the EOP with comparable design parameters [20], the EOP can generate up to approximately 25 kPa under a 250 V driving voltage, which exceeds the $\max \Delta P$ measured from our experiment. This provides both empirical and analytical evidence that supports the bistable behavior of the actuator.

2) Experimental Performance: We then conducted experimental tests to validate the bistable behavior of the actuator. The tested device was fabricated following the design and fabrication procedure described in Section II, where the total transferable working fluid volume was set to V_t = 1100 μL, based on the above analysis. After fabrication, we applied DC voltages below 300 V with opposite polarities to the two ends of the actuator to examine its switching performance between the two stable states. We used a video camera to record the actuator's shape-changing process.

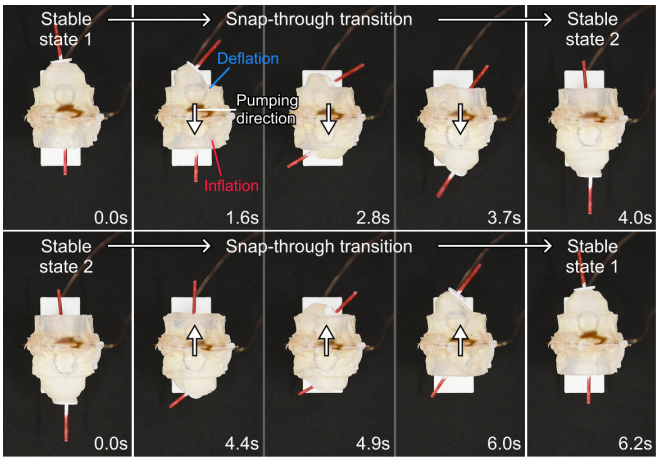

Fig. 4. Experimental validation of the shape-changing process of the BiEOP actuator, where the white arrows show the pumping direction of the working liquid.

Figure 4 presents a representative full shape-changing cycle of the actuator to switch between the two stable states. During the transition from one stable state to the other, one shell undergoes an inflation process while the other experiences deflation, until their shapes are inverted and reach the stable equilibrium point. Once the applied voltage is removed, the actuator remains in the stable configuration. It is worth noting that in this experiment, the switching duration from *State 1* to *State 2* (4.0 s) was shorter than that of the reverse transition (6.2 s). This asymmetry is likely caused by the asymmetry bidirectional pumping pressure generated by the EOP [20]. Moreover, the switching speed of the actuator might be increased by raising the driving voltage, since the flow rate generated by the EOP rises with higher applied voltage [23].

IV. MULTIFUNCTIONAL SOFT ROBOT APPLICATION

In this section, we demonstrate the design of a multifunctional soft robot based on the BiEOP actuators. The robot leverages the bistable characteristics of the BiEOP to reconfigure its body shape, thereby changing the surface conditions that contact the ground to perform two fundamental functions: bristle locomotion and surface adhesion. By coordinating these two functions under different task scenarios, the robot can perform multiple distinct behaviors, including remaining stationary in windy environments, stepping over and picking up flake samples, transporting flake

samples, and attaching to an external movable carrier to assist traveling. We further demonstrate a potential application scenario (Figure 5c), envisioning the use of this soft robot to collect flake samples detached from hard-to-access windy pipes (e.g., contaminated or radioactive), thereby facilitating equipment inspection and maintenance.

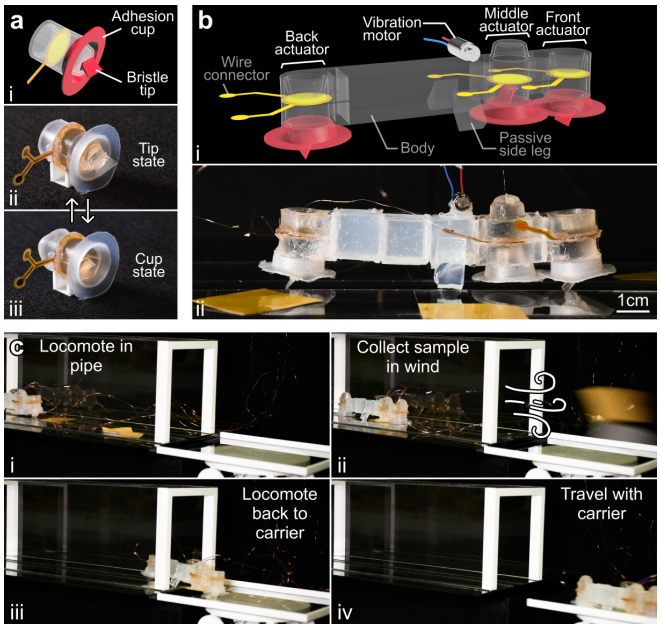

Fig. 5. Multifunctional soft robot design. (a) A modular bistable actuator based on BiEOP that can switch between two contact effectors. (b) Design of the soft robot with three modules that change the contact condition. (c) Application demonstration of the multifunctional soft robot, where it collects and carries flake samples in windy pipes for inspection or maintenance purposes.

A. Design of the Multifunctional Soft Robot

The core component of the robot is a bistable module based on BiEOP that can switch its contact effectors with the ground surface. Here, a BiEOP actuator is modified by gluing two different contact effectors on one of the elastic shells: a soft *adhesion cup* at the outer edge and a rigid *bristle tip* at the center, as shown in Figure 5a. The adhesion cup is fabricated by casting Smooth-On Ecoflex 0030, while the bristle tip is 3D-printed using Clear Resin on a Formlabs Form 3 printer. These two effectors and the BiEOP's bistable configuration determine the module's contact condition with the ground surface.

Specifically, as shown in Figure 5a, when the shell is in the convex stable state, the bristle tip extends out from the adhesion cup to contact the ground, providing a low-friction interface. Due to the bristle tip's asymmetric inclination, it produces slightly different friction forces depending on the module's translation direction, which provides the condition for bristle locomotion when combined with vibrations [25]. Conversely, when the shell is in the concave stable state, the bristle tip retracts along the dome structure and is hidden inside the adhesion cup. In this configuration, the adhesion cup contacts the ground. Due to its large contact area and the material's surface adhesion, it offers the conditions for larger friction and adhesion forces.

The overall robot design integrates three bistable modules introduced above: *front*, *middle*, and *back* actuators, illustrated in Figure 5b. The middle and back actuators are connected via a soft body to maintain balance during locomotion, with passive legs installed on both sides to prevent falling over. Both the soft body and passive legs are cast using Smooth-On Sorta-Clear 12 silicone. An Eccentric Rotating Mass vibration motor (6×10 mm, BestTong) is mounted in the middle, at an empirically determined position that is capable of driving bristle locomotion. All electronic components are connected using 38-gauge fine copper wires to the external power supply and control hardware. The robot has overall dimensions of 12.1 cm in length, 3.7 cm in width, and 3.6 cm in height, and weighs 31.2 g.

We introduce the multiple functions and behaviors enabled by the robot design below.

B. Switch between Bristle Locomotion and Surface Adhesion

By configuring the states of the three bistable modules, we can control the robot's contact conditions with the ground or other surfaces. In our demonstration, we used a glass plate as the ground surface. When only the front and back actuators contact the ground via the bristle tips, the robot exhibits minimal friction force and performs bristle locomotion driven by the vibration motor (Figure 6a). In our test, the static friction force in all directions due to the robot's self-weight was measured to be < 0.01 N, and the robot achieved a maximum translation speed of about 1.8 cm/s with a 2.7 V input to the motor.

When all three modules contact the ground via the adhesion cups, the robot achieves maximum friction and adhesion contact condition (Figure 6b). On the same glass plate, the static friction force under self-weight was measured as 0.33 N, more than 30 times larger than in the bristle-tip configuration. This enabled the robot to remain stationary under challenging conditions, such as a wind speed of approximately 7 m/s, based on our test.

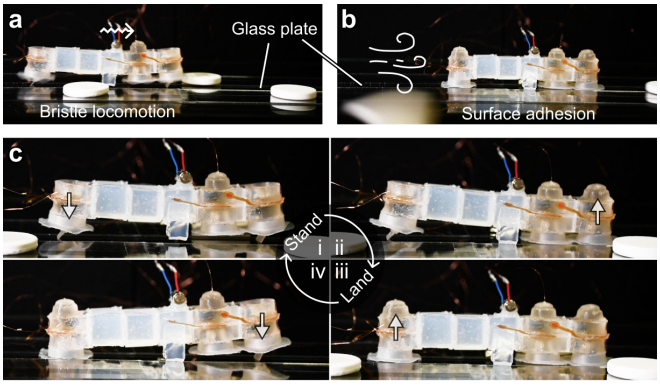

Fig. 6. Function switch between bristle locomotion and surface adhesion. (a) Bristle locomotion function. (b) Surface adhesion function. (c) Switching process between the two functions. The white arrows show the pumping direction of the working liquid.

Figure 6c also illustrates the robot switching process between these two functions, where the robot transitions between *stand* and *land* postures by sequentially changing the configurations of the front and back actuators.

C. Step Over and Pick Up a Flake Sample

By coordinated actuation of the front and middle modules, we first demonstrate the robot stepping over a flake sample. As shown in Figure 7i-iv, when the robot's front tip encounters a thin flake sample that it cannot immediately traverse, it first stops, lowers the middle tip, retracts the front tip, and moves forward, positioning the front actuator above the flake. The robot then stops again, lowers the front tip to step on the flake, and retracts the middle tip. Subsequently, the robot moves forward, allowing the front tip to pass over the flake so that the flake is positioned directly beneath the robot's body.

Then, we demonstrate how the robot picks up the flake sample with the adhesion cup. As shown in Figure 7v-vi, when the flake sample is beneath the middle actuator, the robot can land and attach the flake using the middle adhesion cup. Once the robot returns to a standing posture, the flake is held by the middle adhesion cup and can be transported along with the robot's locomotion.

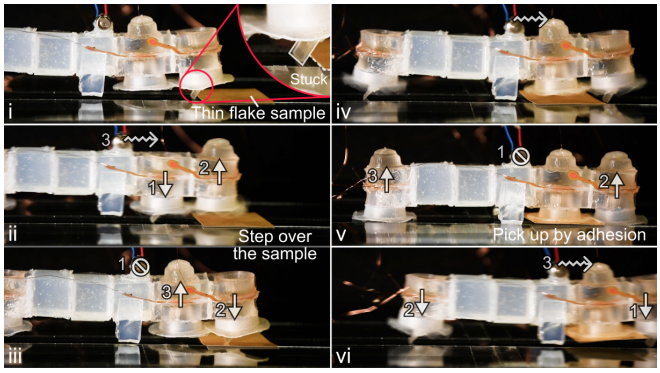

Fig. 7. Step over and pick up a flake sample. The numbers in each figure show the action sequence. The white arrows show the pumping direction of the working liquid.

D. Locomote to Carrier and Travel Together

The robot's surface adhesion function can also be used to attach to an external movable carrier to assist locomotion. As shown in Figure 8, the robot first reaches a movable carrier via bristle locomotion. It then lands on the carrier and attaches itself to the surface using all three adhesion cups, allowing it to move along with the carrier under the effect of static friction. This behavior might help the robot to overcome the limitations of its own locomotion capability. Notably, during this process, the robot can still carry a flake sample using the middle adhesion cup to transport the sample along with the carrier.

E. Application Demonstration

Building on the above robotic behaviors, we further demonstrate an application of flake sample collection in windy pipes. As shown in Figure 5c, the robot first navigates a pipe using bristle locomotion. Upon encountering a flake sample, it steps over and attaches the sample using its adhesion function, and can stabilize itself along with the flake under airflow to prevent disturbance. The robot then carries the sample to a mothership carrier waiting at the pipe outlet, lands on the carrier, and travels alongside it. It could either deliver the sample to an inspector or move to the next pipe entrance for other tasks. We envision the use of such soft robots to collect flake samples from hard-to-access windy pipes (e.g., contaminated or radioactive), thereby facilitating equipment inspection and maintenance.

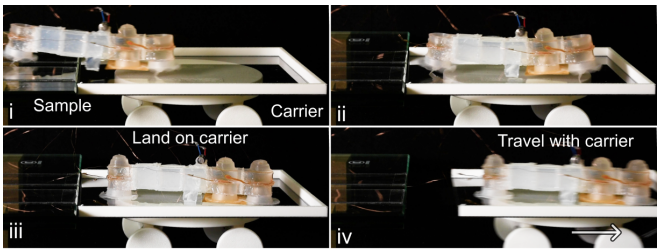

Fig. 8. Locomote to carrier and travel together.

However, the prototypes presented still serve as a proof-of-concept demonstration of the multifunctionality induced by the integrated BiEOP modules in the soft robot, with several open questions remaining for future research. For example, the design of the bristle tip and the vibration module could be further optimized to enhance locomotion speed and stability. The load-bearing capacity of the adhesion cup could also be evaluated, or further improved by optimizing the structural design of the cup module. In addition, exploring untethered implementations of the robot and its performance across diverse environments would broaden its applicability.

V. CONCLUSION

In this work, we present BiEOP, a bistable soft actuator driven by electroosmotic pumps. We analyze and experimentally validate the actuator's bistable behavior based on the pressure–volume characterization of the dome-shaped elastic shell structure within the actuator. We further demonstrate a soft robot that employs BiEOP modules to reconfigure its body shape to switch between bristle locomotion and surface adhesion functions. By collectively utilizing these reconfigurable shapes and functions, the robot can perform diverse behaviors, highlighting its potential for applications such as collecting flake samples detached from hard-to-access windy pipes to assist with equipment inspection and maintenance.

Future work of this project spans several directions. For example, the current EOP may exhibit instability or performance degradation after repeated bidirectional switching. Future efforts could focus on material or control approaches to improve the actuator durability. The geometry of the shell can also be further investigated to achieve different bistable or multistable behaviors. Looking toward future applications,

we envision BiEOP as a modular actuator capable of inducing shape reconfiguration and multifunctionality in the design of future soft robots.

ACKNOWLEDGMENT

We would like to thank all the lab members for their valuable discussions and support throughout the project. We thank Jeremy Chen and Ariel Hong for their suggestions and help with the final demo preparation.

REFERENCES

[1] Y. Cao, M. Derakhshani, Y. Fang, G. Huang, and C. Cao, "Bistable Structures for Advanced Functional Systems," *Advanced Functional Materials*, vol. 31, no. 45, p. 2106231, 2021. [Online]. Available: https://onlinelibrary.wiley.com/doi/abs/10.1002/adfm.202106231

[2] Y. Forterre, J. M. Skotheim, J. Dumais, and L. Mahadevan, "How the Venus flytrap snaps," *Nature*, vol. 433, no. 7024, pp. 421–425, Jan. 2005, publisher: Nature Publishing Group. [Online]. Available: https://www.nature.com/articles/nature03185

[3] Y. Chi, Y. Li, Y. Zhao, Y. Hong, Y. Tang, and J. Yin, "Bistable and Multistable Actuators for Soft Robots: Structures, Materials, and Functionalities," *Advanced Materials*, vol. 34, no. 19, p. 2110384, 2022. [Online]. Available: https://doi.org/10.1002/adma.202110384

[4] S. Shan, S. H. Kang, J. R. Raney, P. Wang, L. Fang, F. Candido, J. A. Lewis, and K. Bertoldi, "Multistable Architected Materials for Trapping Elastic Strain Energy," *Advanced Materials*, vol. 27, no. 29, pp. 4296–4301, 2015. [Online]. Available: https://onlinelibrary.wiley.com/doi/abs/10.1002/adma.201501708

[5] D. Drotman, S. Jadhav, D. Sharp, C. Chan, and M. T. Tolley, "Electronics-free pneumatic circuits for controlling soft-legged robots," *Science Robotics*, vol. 6, no. 51, p. eaay2627, Feb. 2021. [Online]. Available: https://www.science.org/doi/10.1126/scirobotics.aay2627

[6] J. T. B. Overvelde, T. Kloek, J. J. A. D'haen, and K. Bertoldi, "Amplifying the response of soft actuators by harnessing snap-through instabilities," *Proceedings of the National Academy of Sciences*, vol. 112, no. 35, pp. 10 863–10 868, Sept. 2015, publisher: Proceedings of the National Academy of Sciences. [Online]. Available: https://www.pnas.org/doi/full/10.1073/pnas.1504947112

[7] P. Rothemund, A. Ainla, L. Belding, D. J. Preston, S. Kurihara, Z. Suo, and G. M. Whitesides, "A soft, bistable valve for autonomous control of soft actuators," *Science Robotics*, vol. 3, no. 16, p. eaar7986, Mar. 2018, publisher: American Association for the Advancement of Science. [Online]. Available: https://www.science.org/doi/10.1126/scirobotics.aar7986

[8] D. Yang, M. Feng, J. Sun, Y. Wei, J. Zou, X. Zhu, and G. Gu, "Soft multifunctional bistable fabric mechanism for electronics-free autonomous robots," *Science Advances*, vol. 11, no. 5, p. eads8734, Jan. 2025, publisher: American Association for the Advancement of Science. [Online]. Available: https://www.science.org/doi/10.1126/sciadv.ads8734

[9] H. Shahsavan, A. Aghakhani, H. Zeng, Y. Guo, Z. S. Davidson, A. Priimagi, and M. Sitti, "Bioinspired underwater locomotion of light-driven liquid crystal gels," *Proceedings of the National Academy of Sciences*, vol. 117, no. 10, pp. 5125–5133, Mar. 2020, publisher: Proceedings of the National Academy of Sciences. [Online]. Available: https://www.pnas.org/doi/10.1073/pnas.1917952117

[10] Z. Chen, S. Kong, Y. He, S. Chen, W. Wang, L. Jin, S. Zhang, Y. Hong, L. Pan, H. Wu, Y. Xie, C. Linghu, Z. Mao, Z. Yang, C. H. Chan, J. Song, and J. Lu, "A Magnet-Driven Soft Bistable Actuator," *Advanced Functional Materials*, vol. 34, no. 17, p. 2311498, 2024. [Online]. Available: https://onlinelibrary.wiley.com/doi/abs/10.1002/adfm.202311498

[11] Z. Zhakypov, K. Mori, K. Hosoda, and J. Paik, "Designing minimal and scalable insect-inspired multi-locomotion millirobots," *Nature*, vol. 571, no. 7765, pp. 381–386, July 2019, publisher: Nature Publishing Group. [Online]. Available: https://www.nature.com/articles/s41586-019-1388-8

[12] Y. Tang, Y. Chi, J. Sun, T.-H. Huang, O. H. Maghsoudi, A. Spence, J. Zhao, H. Su, and J. Yin, "Leveraging elastic instabilities for amplified performance: Spine-inspired high-speed and high-force soft robots," *Science Advances*, vol. 6, no. 19, p. eaaz6912, May 2020, publisher: American Association for the Advancement of Science. [Online]. Available: https://www.science.org/doi/10.1126/sciadv.aaz6912

[13] D. S. Kim, Y.-J. Lee, Y. B. Kim, Y. Wang, and S. Yang, "Autonomous, untethered gait-like synchronization of lobed loops made from liquid crystal elastomer fibers via spontaneous snap-through," *Science Advances*, vol. 9, no. 20, p. eadh5107, May 2023, publisher: American Association for the Advancement of Science. [Online]. Available: https://www.science.org/doi/10.1126/sciadv.adh5107

[14] D. Lunni, M. Cianchetti, C. Filippeschi, E. Sinibaldi, and B. Mazzolai, "Plant-Inspired Soft Bistable Structures Based on Hygroscopic Electrospun Nanofibers," *Advanced Materials Interfaces*, vol. 7, no. 4, p. 1901310, 2020. [Online]. Available: https://onlinelibrary.wiley.com/doi/abs/10.1002/admi.201901310

[15] Q. Zhao, X. Yang, C. Ma, D. Chen, H. Bai, T. Li, W. Yang, and T. Xie, "A bioinspired reversible snapping hydrogel assembly," *Materials Horizons*, vol. 3, no. 5, pp. 422–428, Aug. 2016, publisher: The Royal Society of Chemistry. [Online]. Available: https://pubs.rsc.org/en/content/articlelanding/2016/mh/c6mh00167j

[16] M. Follador, A. T. Conn, and J. Rossiter, "Bistable minimum energy structures (BiMES) for binary robotics," *Smart Materials and Structures*, vol. 24, no. 6, p. 065037, May 2015, publisher: IOP Publishing. [Online]. Available: https://doi.org/10.1088/0964-1726/24/6/065037

[17] B. D. Iverson and S. V. Garimella, "Recent advances in microscale pumping technologies: a review and evaluation," *Microfluidics and Nanofluidics*, vol. 5, no. 2, pp. 145–174, Aug. 2008. [Online]. Available: https://doi.org/10.1007/s10404-008-0266-8

[18] B. J. Kirby, *Electroosmosis*. Cambridge University Press, 2010, p. 131–152.

[19] P. Rothemund, N. Kellaris, S. K. Mitchell, E. Acome, and C. Keplinger, "HASEL Artificial Muscles for a New Generation of Lifelike Robots—Recent Progress and Future Opportunities," *Advanced Materials*, vol. 33, no. 19, p. 2003375, 2021. [Online]. Available: https://onlinelibrary.wiley.com/doi/abs/10.1002/adma.202003375

[20] T. Yu, P. He, B. T. Wei, C. Wang, X. Li, X. Wang, Y. Lu, W. Yue, M. Teng, Z. Wang, L. Lin, H. Mi, Q. Lu, and L. Yao, "MorphingSkin: A Skin-like Platform that Integrates Multimodal Hydraulic Actuators Based on Flexible Electroosmotic Pumps," in *Proceedings of the 38th Annual ACM Symposium on User Interface Software and Technology*, ser. UIST '25. New York, NY, USA: Association for Computing Machinery, 2025, pp. 1–21. [Online]. Available: https://dl.acm.org/doi/10.1145/3746059.3747685

[21] V. Cacucciolo, J. Shintake, Y. Kuwajima, S. Maeda, D. Floreano, and H. Shea, "Stretchable pumps for soft machines," *Nature*, vol. 572, no. 7770, pp. 516–519, Aug. 2019, number: 7770 Publisher: Nature Publishing Group. [Online]. Available: https://www.nature.com/articles/s41586-019-1479-6

[22] M. Smith, V. Cacucciolo, and H. Shea, "Fiber pumps for wearable fluidic systems," *Science*, vol. 379, no. 6639, pp. 1327–1332, Mar. 2023, publisher: American Association for the Advancement of Science. [Online]. Available: https://www.science.org/doi/10.1126/science.ade8654

[23] C. Shultz and C. Harrison, "Flat Panel Haptics: Embedded Electroosmotic Pumps for Scalable Shape Displays," in *Proceedings of the 2023 CHI Conference on Human Factors in Computing Systems*, ser. CHI '23. New York, NY, USA: Association for Computing Machinery, 2023, pp. 1–16. [Online]. Available: https://dl.acm.org/doi/10.1145/3544548.3581547

[24] T. Yu, Y. Liu, Y. Liu, Q. Lu, T. Han, and H. Mi, "FlexEOP: Flexible Shape-changing Actuator using Embedded Electroosmotic Pumps," in *Adjunct Proceedings of the 37th Annual ACM Symposium on User Interface Software and Technology*, ser. UIST Adjunct '24. New York, NY, USA: Association for Computing Machinery, Oct. 2024, pp. 1–5. [Online]. Available: https://doi.org/10.1145/3672539.3686785

[25] L. V. Nguyen, K. T. Nguyen, and V. A. Ho, "Terradynamics of Monolithic Soft Robot Driven by Vibration Mechanism," *IEEE Transactions on Robotics*, vol. 41, pp. 1436–1455, 2025. [Online]. Available: https://ieeexplore.ieee.org/document/10852184